PCCP

PAPER

View Article Online
View Journal | View Issue

Cite this: *Phys. Chem. Chem. Phys.*, 2016, **18**, 33329

Magnetic coupling in a hybrid Mn(II) acetylene dicarboxylate†

Christopher H. Hendon,*[a] Fabienne Pradaux-Caggiano,[b] Lauren E. Hatcher,[b] William J. Gee,[b] Chick C. Wilson,[b] Keith T. Butler,[b] David R. Carbery,[b] Aron Walsh[c] and Brent C. Melot*[d]

Received 7th October 2016,
Accepted 18th November 2016

DOI: 10.1039/c6cp06886c

www.rsc.org/pccp

The design of ligands that mediate through-bond long range super-exchange in metal–organic hybrid materials would expand chemical space beyond the commonly observed short range, low temperature magnetic ordering. Here we examine acetylene dicarboxylate as a potential ligand that could install long range magnetic ordering due to its spatially continuous frontier orbitals. Using a known Mn(II)-containing coordination polymer we compute and measure the electronic structure and magnetic ordering. In this case, the latter is weak owing to the sub-optimal ligand coordination geometry, with a critical temperature of 2.5 K.

The inherent porosity of metal–organic frameworks (MOFs) has encouraged researchers to focus on heterogeneous applications like gas storage and chemical sensing.[1,2] Besides geometric structure, these materials offer the ability to independently tune the inorganic and organic moieties as a route to design new catalysts, photovoltaic materials, and magnetically ordered frameworks with unparalleled compositional diversity.[3–7] The inclusion of spin-polarised metals in the secondary building unit (SBU)[8] provides access to a variety of exciting electronic[9] and physical properties, including magneto-sensing through changes in magnetic ordering.[10–13] This effect was indirectly presented by Talin *et al.* in their study of HKUST-1 loaded with TCNQ,[14] and later by Kosaka and co-workers showing that TCNQ mediated an antiferromagnetic (AFM) interaction in a Ru-based material.[15] TCNQ has also been used in other studies to mediate magnetic interactions.[16] The origin of these changes in magnetic interactions are attributed to the energy level matching of TCNQ with many of the late-transition metal highest energy electrons.[17] However, these properties are not limited to TCNQ, as there are countless other examples in the literature where magnetic structure is modulated through guest inclusion.[18,19]

The magnetic structure of MOFs and other hybrid solids are determined by both the chemistry of the bridging ligand and the identity of the metal. In the Cu-containing HKUST-1,[20] two Cu^{2+} atoms are AFM coupled through a super-exchange interaction, Fig. 1a. In the archetypal AFM coupled material, MnO, the Mn^{2+} demonstrate strong AFM interactions across the bridging oxo 'ligand', through a so-called super-exchange interaction (Fig. 1b).[21] Strong super-exchange interactions are typically

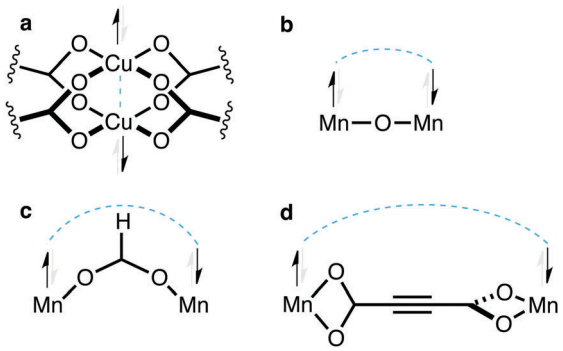

Fig. 1 Spin-polarised metals may magnetically order through either direct exchange interactions, or longer-range super-exchange. Here the coupled metals are shown linked by a blue dotted line, and the electronic spin is simplified to a single electron (black), with the exchanged electron schematically represented in light grey. The strongest magnetic interaction, short range exchange is shown in (a), an example of which is found in Cu–Cu paddlewheels like that of cupric acetate. This deviates from the super-exchange interactions because the metals are coupled through space, rather than through bond. The quintessential super-exchange material, MnO shown in (b), exhibits longer range ordering mediated by the bridging oxide. Longer again is that of the formate bridge metals, (c). Here, we are interested in mediating the magnetic coupling between metals through the helical orbitals associated with acetylene dicarboxylate, (d).

[a] *Department of Chemistry, Massachusetts Institute of Technology, Cambridge, MA, 02139, USA. E-mail: hendon@mit.edu; Web: www.twitter.com/chhendon*
[b] *Department of Chemistry, University of Bath, Bath, BA2 7AY, UK*
[c] *Department of Materials, Imperial College London, Exhibition Road, London, SW7 2AZ, UK*
[d] *Department of Chemistry, University of Southern California, Los Angeles, CA, 90089, USA. E-mail: melot@usc.edu*

† Electronic supplementary information (ESI) available: χ^{-1} *vs.* T plot. CCDC 1484654. For ESI and crystallographic data in CIF or other electronic format see DOI: 10.1039/c6cp06886c

limited to dense materials where either (i) the metals are in close proximity as demonstrated in MnO (d(Mn–Mn) = 4.50 Å) or (ii) the metals are bridged by a closed shell oxide/chalcogenide.[22,23] To design a material with longer-range super-exchange coupling through an organic ligand is more challenging: the coupling energy decreases rapidly as the metals become spatially separated and electronic structure of the ligand plays an increasingly pivotal role. Because the magnetic structure is intimately related to the interface between the metal and ligand, *a priori* design of strong long-range magnetic ordering is infrequently observed in the literature. For example, there are reports of Co-[24–26] and Fe-containing[27,28] materials that demonstrated strong coupling, but these interactions are mediated through space, rather than through bond: larger ligands usually are of detriment to metal–metal interactions.

The formate ligand has seen some success in extending the bridging distance between spin polarised metals (Fig. 1c).[29] Some examples include Mn^{2+}, Fe^{2+} and Cu^{2+} in perovskite-like structures:[30–32] the structural library of MOFs is limited to perovskite-like structure types, but they are frequently observed due to their predictable orientation and high resultant crystal density.[33] Yet, long-range magnetic coupling in hybrid materials remains a challenge, as the interaction energy is determined by orbital symmetry of the ligand.[34] The ligand plays a crucial role in creating novel magnetic hybrid materials, and their realization would provide the foundation for an interesting class of materials.

Recently, we reported an electronic structure study of unusual helical and spatially continuous orbitals[35] present in both the HOMO and LUMO acetylene dicarboxylate (ACDC), and other linear carbon-rich molecules.[36,37] We later postulated that these ligands could mediate high temperature long range magnetic ordering (our example was through the formation of 1D chains with general formula –Mn–ACDC–Mn–, Fig. 1d).[38] The origin of this was attributed to favorable orbital symmetry interactions between metal and ligand, mediated by the spatially continuous ligand centered helical orbital. With no previous reports of magnetic ordering in Mn–ACDC containing materials, we sought to synthesize our theoretical 1D chain complexes.

The synthesis of pure phase hybrid solid materials is challenging, with entropic effects playing a significant role in the final crystal structure.[33,39] Initial attempts at forming a crystalline material focused on mixing $Mn(OAc)_2$ and acetylene dicarboxylic acid solely in methanol. However, rapid formation of amorphous and microcrystalline solids were observed. To address this issue, the adoption of an initial biphasic water/methanol medium led to the formation of crystalline material suitable for single crystal X-ray crystallographic analysis (complete synthetic details are presented at the end of the paper). Single crystal X-ray diffraction was used to determine the absolute structure of the colorless crystals. Indeed, we failed at isolating the hypothetical 1D chain complex. Instead the material crystallized the historically reported structure presented in Fig. 2a,[40] in the monoclinic space group $C2/c$ (a = 13.4976 Å, b = 7.1793 Å, c = 7.8799 Å, β = 123.4050° at 100 K). It should be noted that this is just one of numerous possible structures containing at minimum Mn^{2+} and the ACDC linker. In this structure, the Mn^{2+} centers

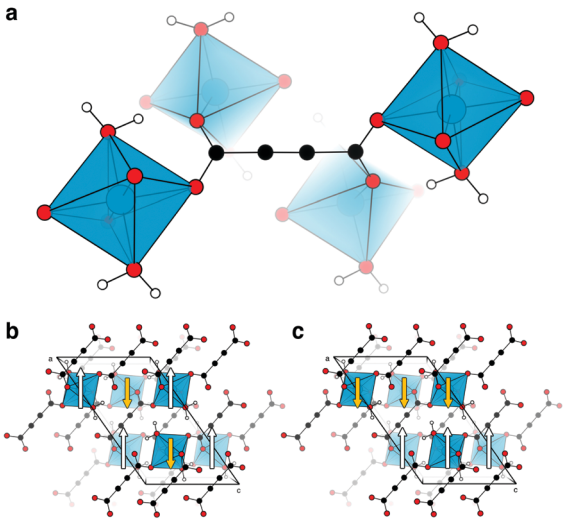

Fig. 2 Mn–ACDC features the connectivity shown in (a), where each ACDC ligand links four Mn^{2+} ions that are all within 5 Å to 6 Å of each other. This gives rise to two possible magnetic orderings in the unit cell: a short range antiferromagnetic (AFM_{SR}) orientation, (b), which permits all Mn^{2+} centers to be AFM relative to each other, and a long range antiferromagnetic (AFM_{LR}) orientation where carboxylate bridge Mn^{2+} are ferromagnetically (FM) arranged, and ACDC-bridged Mn^{2+} centers are AFM, (c).

adopt an octahedral coordination geometry with four unique equatorial ACDC ligands and two axial H_2O molecules. The ACDC ligands coordinate to the Mn^{2+} in the *syn–anti* mode, which is favourable for formate-like bridged coupling, but less ideal for through-ligand ordering. There are four distinct Mn–Mn distances; the carboxylate bridges species (d(Mn–Mn) = 5.33 Å), the *syn–syn* through-ligand couple (d(Mn–Mn) = 9.87 Å) the *syn–anti* through ligand couple (d(Mn–Mn) = 7.87 Å) and the *anti–anti* through-ligand couple (d(Mn–Mn) = 5.64 Å).

The Mn–ACDC coordination polymer features I^0O^3 connectivity,[41] where adjacent Mn^{2+} are chemically connected in three dimensions through ACDC. These units arrange in a pseudo-layered topology that results in each Mn-center having two nearest neighbor interactions within the plane that are mediated through super-superexchange (*i.e.* through the ACDC alkyne) and two next-nearest neighbor distances out of plane (*i.e.* through the ACDC carboxylic acid motif). Limiting the possible magnetic arrangements to a single crystallographic unit cell, there are two possible AFM orientations: a short range AFM arrangement, or checkerboard ordering (Fig. 2b), and a long range AFM interaction, or striped ordering (Fig. 2c).

Through serendipity, this Mn–ACDC structure is of more general interest because there are two competing AFM arrangements that can be isolated, Fig. 2b and c. In any case, we decided to perform our magnetic measurements on this material to determine if (i) the ACDC ligand still permitted long range magnetic ordering and (ii) whether the competition between the two AFM arrangements were in competition, thereby negating magnetic ordering.

To assess the magnetic structure, a combined DFT and magnetism experimental approach was taken. Using the computational methods described herein, the total energies of the

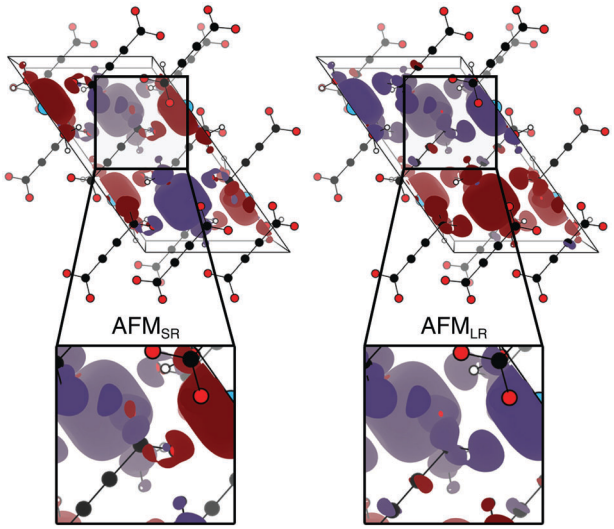

Fig. 3 The spin densities of the AFM_{SR} (left) and AFM_{LR} (right). Spin channel 1 is shown in red, and spin channel 2 in purple. AFM_{SR} features a formate-like bridge where the spin channels interact, permitting coupling across the carboxylate bridge with no contribution from the alkyne region of ACDC. Conversely, the AFM_{LR} orientation shows a FM interaction between carboxylate-bridge metal centres, and spin contributions along the alkyne-chain; a weak but significant long range super-exchange interaction.

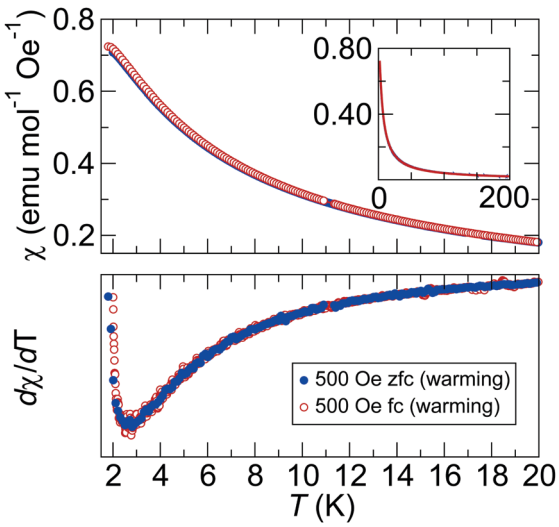

Fig. 4 Top panel: Temperature-dependent magnetic susceptibility of Mn–ACDC collected as zero-field-cooled (filled blue dots) and field-cooled (unfilled red dots) near the ordering temperature of 2.5 K. The inset shows a wider temperature range in order to illustrate the Curie–Weiss behavior. Bottom panel: Derivative of the magnetization with respect to the temperature, clearly showing a point of inflection in the data around 2.5 K.

AFM_{SR}, AFM_{LR} and FM structure were compared (Fig. 3). The computed coupling constants were $AFM_{SR} = -0.035$ meV and $AFM_{LR} = -0.015$ meV relative to the ferromagnetic state, suggesting the Mn^{2+} are antiferromagnetically coupled in the DFT ground state, with the minimum energy configuration corresponding to the formate-bridged checkerboard ordering. The resultant computed Néel temperatures are 7 K and 3 K for the checkerboard and striped, respectively. Spin densities for the short and long range AFM interactions are shown in Fig. 3.

Unlike our previous prediction of Néel temperatures above liquid nitrogen for the theoretical hydrated 1D Mn–ACDC–Mn material, the experimentally realized structure does not feature strong interactions between the spins. This can be attributed to the less-desirable coordination environment that results from the ACDC and Mn^{2+}. From the Goodenough–Kanamori rules, Mn–ACDC does not feature the ideal 180° Mn–ligand–Mn bond angle, and here the Mn e_g ligand field combination does not effectively overlap with the oxide 2p orbitals.[42,43] However, the AFM_{LR} is also relatively disfavored due to a local electronic effect. AFM_{LR} installs a local short range FM interaction which is destabilising. However, examining the computed AFM_{LR} spin density shown in Fig. 3, there is clearly some orbital contribution along the ligand, therefore promoting the long range AFM interaction.

In order to test the theoretically predicted magnetic interactions, the temperature-dependent susceptibility, χ, was collected under a constant dc field of 500 Oe (χ^{-1} *vs.* T is presented in the ESI†). As seen in the inset of the top panel of Fig. 4, Mn–ACDC exhibits the usual inverse relationship between temperature and susceptibility expected from a material with strongly localized magnetic moments. At temperatures approaching 2.5 K a subtle kink in the susceptibility can be seen that suggests the spins begin to adopt an ordered configuration. This point of inflection is more clearly visible in the derivative, $d\chi/dT$, shown in the bottom panel of Fig. 4. Very little divergence is seen between the zero-field-cooled and the field-cooled data, suggesting that the arrangements that the spins adopt are well-ordered and they do not exhibit any disordered or glassy behavior.

The high temperature region (280–150 K) of the magnetic susceptibility was fit to the Curie–Weiss Equation in order to gain more insight into the nature of the magnetic interactions that the ACDC ligand mediates. The effective moment was found to be 5.71 μ_B, in good agreement with the expected value of 5.92 μ_B for a octahedrally coordinated, high-spin, Mn^{2+} ion ($S = 5/2$, $L = 0$) with spin-only contributions to the magnetization $\left[\mu_{(S)} = 2\sqrt{S(S+1)}\right]$. From this fit, θ_{CW} was found to be −6.5 K where the negative sign reflects the dominant antiferromagnetic coupling. Comparing the experimentally determined Curie–Weiss ordering temperature with the computationally predicted ones supports the AFM_{SR} arrangement of the moments as the favored configuration.

The stability of the antiferromagnetic ground state was interrogated by collecting the high-field magnetization curves at 2 K shown in Fig. 5. For small fields up to ±3 T the usual linear response expected for an antiferromagnet is seen; however, it is very clear that fields approaching 6 T onward begin to show saturation at the expected value of 5 μ_B/Mn^{2+} ion. The shape of the magnetization curve bears some similarity to the Brillouin-like response for a fully disordered paramagnetic phase, so a comparison between the two is shown in the top panel of Fig. 5 where a much wider and more pronounced linear region can be seen clearly in the experimental data. A closer examination of the derivative with respect to the field (bottom panel of Fig. 5) reveals a symmetric feature peaking at

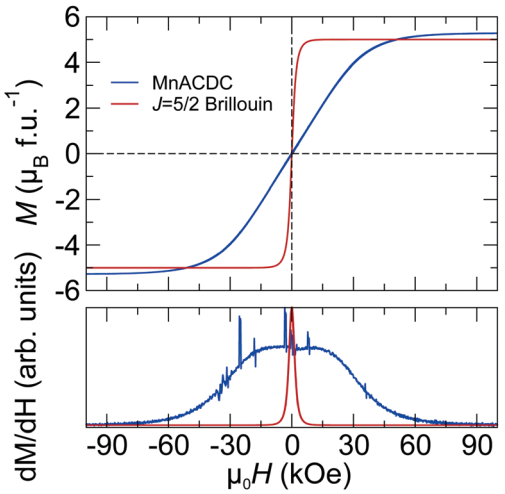

Fig. 5 Top panel: Isothermal magnetization curve collected for Mn–ACDC at 2 K (blue curve) compared to the Brillouin function calculated curve for a J = 5/2 paramagnetic phase (red curve). Bottom panel: Derivative of the magnetization with respect to the field illustrating the field-induced magnetic transition that occurs around 1.5 T in Mn–ACDC.

±1.5 T that most likely corresponds to a field-induced breaking of the antiferromagnetic order in favor of a ferromagnetic arrangement with the moments saturating around 6 T. Given the calculated value for J_{SR} of −0.035 meV is fairly weak, it is reasonable that a field of 1.5 T would be sufficient to force a realignment of the moments into a ferromagnetic orientation.

Given the subtle nature of the magnetism seen here, it is important to note that without a full Curie–Weiss analysis the onset of magnetic order and the field-induced transition would have been easily overlooked. It is fairly common to invoke χT plots in order to analyze the nature of the magnetic order in metal–organic hybrids.[44,45] While this is perfectly valid for small molecules where the implicit assumption is that no collective interaction exists between the magnetic centers, this type of analysis is not appropriate for materials that are capable of coupling through complex superexchange pathways mediated by the organic ligand. Our results clearly demonstrate the importance of not just the organic ligands, but also how they coordinate and subsequently rehybridize with the orbitals on the metal in order to mediate the interactions between the magnetic moments in metal–organic hybrids. In this particular instance, the ACDC ligand did not orientate in the fashion we had hoped, and the magnetic ordering is very weak. Given the high precision in typical DFT calculations we can conclude that this suppression in ordering is likely due to a frustration installed by the geometry imposed by the ACDC ligand. Simply incorporating highly conjugated organic ligands into a framework is not sufficient to ensure strong magnetic or electronic interactions between adjacent metal centers, and the experimental community should focus carefully on developing methods to control or template the crystallization of new hybrid materials. Further work on incorporation of the ACDC ligand is required to obtain a structure with remarkable Néel temperatures.

Synthesis of Mn–ACDC: A solution of acetylene dicarboxylic acid (95% purity, Sigma Aldrich) dissolved in MeOH (2 mL, 0.18 mol L^{-1}) was carefully layered over a solution of $Mn(OAc)_2$ (98% purity, Sigma Aldrich) dissolved in water (2 mL, 0.18 mol L^{-1}) at room temperature. The vial was capped and crystals of the desired Mn–ACDC were harvested after 3 weeks. Mn–ACDC was structurally identical to that previous reported.[40]

Single-crystal details: Data for Mn–ACDC was collected on a Bruker Apex2 CCD diffractometer at 100(2) K using synchrotron radiation (λ = 0.7749 Å) at Station 11.3.1 of the Advanced Light Source, Berkeley. The diffraction data was integrated using APEX2 software,[46] a multiscan adsorption correction was applied using SADABS,[47] and refined by full-matrix least squares on F2 using SHELXL. Crystal data for Mn–ACDC: $C_4H_4MnO_6$ (M = 203.1 g mol^{-1}): monoclinic, space group $C2/c$ (no. 15), crystal size: 0.020 × 0.020 × 0.010 mm^3, a = 13.4976(8) Å, b = 7.1793(4) Å, c = 7.8799(5) Å, β = 123.405(2)°, V = 637.44(7) $Å^3$, Z = 4, ν = 2.573 mm^{-1}, $D_{calc.}$ = 2.115 g cm^{-3}, 4229 reflections measured (7.338° ≤ 2Θ ≤ 57.934°), 649 unique (R_{int} = 0.0370, R_{sigma} = 0.0231) which were used in all calculations. The final R_1 was 0.0174 ($I > 2\sigma(I)$) and wR_2 was 0.0462 (all data). CCDC 1484654 (Mn–ACDC).

Magnetism details: Temperature- and field-dependent magnetic susceptibility data was collected from room temperature to 2 K and up to fields of ±14 T using the Vibrating Sample Magnetometer attachment on a Quantum Design DynaCool Physical Property Measurement system. Powders of the hybrid were kept in their mother liquor until a few moments prior to placing them inside a plastic cap that was firmly sealed in order to prevent rotation of the particles at high fields.

Computational details: Electronic structure calculations were performed within the DFT construct as implemented in the Vienna *ab initio* simulation package (VASP),[48] a plane-wave basis set code (with PAW scalar-relativistic pseudopotentials). A 500 eV plane-wave cutoff and a 2 × 4 × 4 k-grid was employed for electronic convergence to within 0.005 eV per atom. Beginning with the experimentally determined crystallographic cell, all unit cell vectors and internal ionic positions were relaxed to their equilibrium values using the PBEsol[49] functional followed by further structural optimisation with the HSE06 functional.[50,51] Here we perform geometry optimisation at the hybrid function level as the difference in energies very small and small perturbations in the structure can significantly alter the energetics.[52–54] The HSE06 functional features 25% of the short-range semi-local exchange replaced by the non-local Hartree–Fock exchange. The minimum energy electronic structure was obtained with an spin-unrestricted geometry optimisation and was found to be the antiferromagnetically ordered arrangement shown in Fig. 3 (short range). The long range and ferromagnetic states were then enforced and the structures were optimized with these electronic structure parameters kept constant. From these calculations we recover electronic properties including electron density, band gap and magnetic coupling energies.

Acknowledgements

BCM gratefully acknowledges support from the Office of Naval Research Grant # N00014-15-1-2411. The work at the University of Bath benefited by financial support from EPSRC

(Grants EP/I033459/1, EP/J017361/1, EP/K004956/1WK, EP/M009580/1, EP/L000202), the Royal Society, the ERC (Grant 277757) and the Leverhulme Trust. This work used the Extreme Science and Engineering Discovery Environment (XSEDE), which is supported by National Science Foundation grant number ACI-1053575.

References

1 C. E. Wilmer, M. Leaf, C. Y. Lee, O. K. Farha, B. G. Hauser, J. T. Hupp and R. Q. Snurr, *Nat. Chem.*, 2011, **4**, 83–89.
2 S.-J. Lee and Y.-S. Bae, *J. Phys. Chem. C*, 2014, **118**, 19833.
3 S. S. Park, E. R. Hontz, L. Sun, C. H. Hendon, A. Walsh, T. Van Voorhis and M. Dincă, *J. Am. Chem. Soc.*, 2015, **137**, 1774.
4 V. Stavila, A. A. Talin and M. D. Allendorf, *Chem. Soc. Rev.*, 2014, 5994.
5 W. Zhang and R.-G. Xiong, *Chem. Rev.*, 2012, **112**, 1163.
6 Y. Cui, Y. Yue, G. Qian and B. Chen, *Chem. Rev.*, 2012, **112**, 1126.
7 K. T. Butler, C. H. Hendon and A. Walsh, *J. Am. Chem. Soc.*, 2014, **136**, 2703.
8 E. Coronado and G. Mnguez Espallargas, *Chem. Soc. Rev.*, 2013, **42**, 1525.
9 C. H. Hendon, A. Walsh, N. Akiyama, Y. Konno, T. Kajiwara, T. Ito, H. Kitagawa and K. Sakai, *Nat. Commun.*, 2016, **7**, 11950.
10 R. Sibille, E. Lhotel, T. Mazet, B. Malaman, C. Ritter, V. Ban and M. François, *Phys. Rev. B: Condens. Matter Mater. Phys.*, 2014, **89**, 104413.
11 P. Canepa, Y. J. Chabal and T. Thonhauser, *Phys. Rev. B: Condens. Matter Mater. Phys.*, 2013, **87**, 094407.
12 K. Liu, X. Zhang, X. Meng, W. Shi, P. Cheng and A. K. Powell, *Chem. Soc. Rev.*, 2016, **45**, 2423–2439.
13 A. Walsh, K. T. Butler and C. H. Hendon, *MRS Bull.*, 2016, **41**, 870.
14 A. A. Talin, A. Centrone, A. C. Ford, M. E. Foster, V. Stavila, P. Haney, R. A. Kinney, V. Szalai, F. E. Gabaly, H. P. Yoon, F. Léonard and M. D. Allendorf, *Science*, 2014, **343**, 66.
15 W. Kosaka, H. Fukunaga and H. Miyasaka, *Inorg. Chem.*, 2015, **54**, 10001.
16 H. Miyasaka, C. Campos-Fernández, R. Clérac and K. Dunbar, *Angew. Chem., Int. Ed.*, 2000, **112**, 3989.
17 C. H. Hendon and A. Walsh, *Chem. Sci.*, 2015, **6**, 3674.
18 F. Gandara, N. Snejko, A. D. Andres, J. R. Fernandez, J. C. Gomez-Sal, E. Gutierrez-Puebla and A. Monge, *RSC Adv.*, 2012, **2**, 949.
19 L. Peng, J. Zhang, Z. Xue, B. Han, X. Sang, C. Liu and G. Yang, *Nat. Commun.*, 2014, **5**, 4465.
20 S. S. Chui, S. M. Lo, J. P. H. Charmant, A. G. Orpen and I. D. Williams, *Science*, 1999, **283**, 1148.
21 T. M. Wilson, *J. Appl. Phys.*, 1969, **40**, 1588.
22 P. T. Barton, M. C. Kemei, M. W. Gaultois, S. L. Moffitt, L. E. Darago, R. Seshadri, M. R. Suchomel and B. C. Melot, *Phys. Rev. B: Condens. Matter Mater. Phys.*, 2014, **90**, 064105.
23 B. C. Melot, A. Goldman, L. E. Darago, J. D. Furman, E. E. Rodriguez and R. Seshadri, *J. Phys.: Condens. Matter*, 2010, **22**, 506003.
24 P. J. Saines, P. T. Barton, M. Jura, K. S. Knight and A. K. Cheetham, *Mater. Horiz.*, 2014, **1**, 332.
25 K. L. Svane, P. J. Saines and A. Walsh, *J. Mater. Chem. C*, 2015, **3**, 11076.
26 S. Xiang, X. Wu, J. Zhang, R. Fu, S. Hu and X. Zhang, *J. Am. Chem. Soc.*, 2005, **127**, 16352.
27 H. Lu, T. Yamamoto, W. Yoshimune, N. Hayashi, Y. Kobayashi, Y. Ajiro and H. Kageyama, *J. Am. Chem. Soc.*, 2015, **137**, 9804.
28 S. Goswami, A. Adhikary, H. S. Jena, S. Biswas and S. Konar, *Inorg. Chem.*, 2013, **52**, 12064.
29 B. Z. Wang, K. Hu, S. Gao and H. Kobayashi, *Adv. Mater.*, 2010, **22**, 1526–1533.
30 A. K. Cheetham and C. N. R. Rao, *Science*, 2007, **318**, 58.
31 Z. Wang, P. Jain, K. Y. Choi, J. Van Tol, A. K. Cheetham, H. W. Kroto, H. J. Koo, H. Zhou, J. Hwang, E. S. Choi, M. H. Whangbo and N. S. Dalal, *Phys. Rev. B: Condens. Matter Mater. Phys.*, 2013, **87**, 224406.
32 Y. Tian, W. Wang, Y. Chai, J. Cong, S. Shen, L. Yan, S. Wang, X. Han and Y. Sun, *Phys. Rev. Lett.*, 2014, **112**, 17202.
33 G. Kieslich, S. Kumagai, K. T. Butler, T. Okamura, C. H. Hendon, S. Sun, M. Yamashita, A. Walsh and A. K. Cheetham, *Chem. Commun.*, 2015, **51**, 15538–15541.
34 F. A. Almeida Paz, J. Klinowski, S. M. F. Vilela, J. P. C. Tomé, J. A. S. Cavaleiro and J. Rocha, *Chem. Soc. Rev.*, 2012, **41**, 1088.
35 C. H. Hendon, D. Tiana, A. T. Murray, D. R. Carbery and A. Walsh, *Chem. Sci.*, 2013, **4**, 4278.
36 E. Soriano and I. Fernández, *Chem. Soc. Rev.*, 2014, **43**, 3041.
37 F. Diederich, P. J. Stang and R. R. Tykwinski, *Acetylene Chemistry: Chemistry, Biology and Material Science*, John Wiley & Sons, 2006.
38 D. Tiana, C. H. Hendon and A. Walsh, *Chem. Commun.*, 2014, **50**, 13990.
39 K. T. Butler, A. Walsh, A. K. Cheetham and G. Kieslich, *Chem. Sci.*, 2016, **7**, 6316–6324.
40 C. Robl and S. Hentschel, *Z. Anorg. Allg. Chem.*, 1990, **591**, 188–194.
41 A. K. Cheetham, C. Rao and R. K. Feller, *Chem. Commun.*, 2006, 4780.
42 J. B. Goodenough, *Magnetism and chemical bond*, Interscience Publ., 1963, vol. 1.
43 A. J. Tasiopoulos, A. Vinslava, W. Wernsdorfer, K. A. Abboud and G. Christou, *Angew. Chem., Int. Ed.*, 2004, **116**, 2169.
44 J. A. DeGayner, I.-R. Jeon and T. D. Harris, *Chem. Sci.*, 2015, **6**, 6639.
45 M. Kurmoo, *Chem. Soc. Rev.*, 2009, **38**, 1353.
46 *APEX2, v2014.9-0*, Bruker AXS Inc., Madison, WI, USA, 2014.
47 *SADABS Program for Empirical Absorption Correction and Scaling of X-ray Data*, Bruker AXS Inc., Madison, WI, USA, 2005.
48 G. Kresse and J. Furthmüller, *Phys. Rev. B: Condens. Matter Mater. Phys.*, 1996, **54**, 11169.
49 J. P. Perdew, A. Ruzsinszky, G. I. Csonka, O. A. Vydrov, G. E. Scuseria, L. A. Constantin, X. Zhou and K. Burke, *Phys. Rev. Lett.*, 2008, **100**, 136406.

50 J. Heyd, G. E. Scuseria and M. Ernzerhof, *J. Chem. Phys.*, 2003, **118**, 8207.
51 A. V. Krukau, O. A. Vydrov, A. F. Izmaylov and G. E. Scuseria, *J. Chem. Phys.*, 2006, **125**, 224106.
52 A. J. Jackson, J. M. Skelton, C. H. Hendon, K. T. Butler and A. Walsh, *J. Chem. Phys.*, 2015, **143**, 184101.
53 M. B. Chambers, X. Wang, N. Elgrishi, C. H. Hendon, A. Walsh, J. Bonnefoy, J. Canivet, E. A. Quadrelli, D. Farrusseng, C. Mellot-Draznieks and M. Fontecave, *ChemSusChem*, 2015, **8**, 603.
54 C. H. Hendon, K. E. Wittering, T.-H. Chen, W. Kaveevivitchai, I. Popov, K. T. Butler, C. C. Wilson, D. L. Cruickshank, O. Š. Miljanić and A. Walsh, *Nano Lett.*, 2015, **15**, 2149.

